

# We are IntechOpen, the world's leading publisher of Open Access books Built by scientists, for scientists

4,800

Open access books available

122,000

International authors and editors

135M

Downloads

Our authors are among the

154

Countries delivered to

TOP 1%

most cited scientists

12.2%

Contributors from top 500 universities



WEB OF SCIENCE™

Selection of our books indexed in the Book Citation Index  
in Web of Science™ Core Collection (BKCI)

Interested in publishing with us?  
Contact [book.department@intechopen.com](mailto:book.department@intechopen.com)

Numbers displayed above are based on latest data collected.  
For more information visit [www.intechopen.com](http://www.intechopen.com)



## Chapter

# The Cobalt Oxide-Based Composite Nanomaterial Synthesis and Its Biomedical and Engineering Applications

*Lingala Syam Sundar, Manoj K. Singh, António M.B. Pereira and Antonio C.M. Sousa*

## Abstract

The magnetic nanoparticles (NPs) are offering a wide range of applications in medical and engineering fields. Among all the magnetic nanoparticles, cobalt oxide ( $\text{Co}_3\text{O}_4$ ) nanoparticles and its composite-based nanoparticles are attracting more interest from researchers because of its unique mechanical, thermal, and magnetic properties. The aim of this book is to bring together a number of recent contributions regarding the cobalt oxide-based composite nanoparticles from several researchers all over the world. The latest research results, innovations, and methodologies are reported in the book in order to support the discussion and to circulate ideas and knowledge about the applications of these materials in medical and engineering applications. This chapter presents the methodology for the synthesis and characterization and applications of cobalt oxide-based composite nanoparticles. The detailed analysis related to toxicity of these nanocomposite materials is also included in this book chapter.

**Keywords:** cobalt oxide, nanocomposite, thermal properties, electrical properties and toxicity

## 1. Introduction

Magnetic nanoparticles (NPs) are attracting increased researchers' interest due to their potential wide use in many engineering and medical applications. The most commonly used magnetic materials are  $\text{Fe}_2\text{O}_3$ ,  $\text{Fe}_3\text{O}_4$ , Ni, Co, CoO, and  $\text{Co}_3\text{O}_4$ . However, among all these magnetic materials, cobalt oxide ( $\text{Co}_3\text{O}_4$ ) nanoparticles are being preferred due to their good magnetic properties. Pure cobalt is not stable at room temperature as it can be converted to oxides like CoO,  $\text{Co}_2\text{O}_3$ , and  $\text{Co}_3\text{O}_4$ ;  $\text{Co}_3\text{O}_4$  is the most stable phase. It is a P-type semiconductor, and it has high Young's modulus, which varies between 116 and 160 GPa.  $\text{Co}_3\text{O}_4$  exhibits a normal spinel crystal structure with occupation of tetrahedral sites by  $\text{Co}^{2+}$  and octahedral sites by  $\text{Co}^{3+}$ . Its magnetic moment arises due to  $\text{Co}^{2+}$  ions largely because of spins, with a small contribution from spin-orbit coupling.  $\text{Co}_3\text{O}_4$  has excellent properties such as gas-sensing, catalytic, and electrochemical properties, and it has been studied

widely for applications in solid-state sensors, electrochromic devices, and heterogeneous catalysts as well as lithium batteries and also medical applications [1–5]. There are several methods to synthesize the  $\text{Co}_3\text{O}_4$  nanoparticles, which include the  $\text{Co}_3\text{O}_4$  nanowires [6], the surfactant-templated approach for fabricating  $\text{Co}_3\text{O}_4$  nanoboxes [7], the mechanochemical reaction method for the synthesis of  $\text{Co}_3\text{O}_4$  nanoparticles [8], the thermal decomposition and oxidation route for the growth of  $\text{Co}_3\text{O}_4$  nanorods [9], and the  $\text{Co}_3\text{O}_4$  nanowalls [10].

Some of the reports dealing with the synthesis of  $\text{Co}_3\text{O}_4$  nanoparticles and their potential use are succinctly reviewed below. Manigandan et al. [11] used the thermal decomposition method. Mariano et al. [12] synthesized  $\text{Co}_3\text{O}_4$  nanoparticles and prepared ethylene glycol-based nanofluids. Salavati-Niasari et al. [13] prepared  $\text{Co}_3\text{O}_4$  nanoparticles from solid organometallic molecular precursors. Salavati-Niasari et al. [14] used another method by considering benzene dicarboxylate complexes, in particular phthalate ones, as precursors. Alrehaily et al. [15] synthesized  $\text{Co}_3\text{O}_4$  nanoparticles by gamma irradiation. All the above researchers synthesized the  $\text{Co}_3\text{O}_4$  nanoparticles for engineering applications. Cavallo et al. [16] studied the cytotoxicity of  $\text{Co}_3\text{O}_4$  nanoparticles in human alveolar (A549) and bronchial (BEAS-2B) cells. Alarifi et al. [17] investigated the toxicity of  $\text{Co}_3\text{O}_4$  nanoparticles in HepG2 cells. Based on these studies, pure  $\text{Co}_3\text{O}_4$  nanoparticles are toxic.

Cobalt-based compounds also offer interesting advantages in various applications; typical cobalt-based compounds are grapheme oxide/cobalt oxide, nanodiamond-cobalt oxide, zeolite Y/cobalt oxide, and carbon nanotubes/cobalt oxide. Syam Sundar et al. [18] synthesized GO/ $\text{Co}_3\text{O}_4$  hybrid nanoparticles and studied their thermal properties. Syam Sundar et al. [19] also synthesized ND- $\text{Co}_3\text{O}_4$  nanoparticles and investigated their thermal properties and toxicity. Shi et al. [20] prepared different concentrations of  $\text{Co}_3\text{O}_4$ /GO, studied their catalyst activity, and observed the highest catalytic activity when the  $\text{Co}_3\text{O}_4$  mass loading was about 50% in the catalyst. Xiang et al. [21] synthesized rGO/ $\text{Co}_3\text{O}_4$ , which was used as the pseudocapacitor electrode in the 2 M KOH aqueous electrolyte solution.

This book chapter emphasizes on the various synthesis methods for cobalt oxide and engineering and medical applications of this material. In addition, synthesis, characterization, and engineering and medical applications of cobalt oxide-based composite materials are also reviewed.

## 2. Cobalt oxide ( $\text{Co}_3\text{O}_4$ ) nanoparticles

### 2.1 Synthesis procedure

There are different methods to synthesize  $\text{Co}_3\text{O}_4$  nanoparticles, which, among others, are chemical coprecipitation, mechanochemical reaction, thermal decomposition and oxidation route, and long-time calcining method. Manigandan et al. [11] used thermal decomposition method for the synthesis of  $\text{Co}_3\text{O}_4$  nanoparticles by dispersing 0.01 M cobalt chloride in 500 mL distilled water and 10% of glycerol. The suspension was stirred for 20 min by a magnetic stirrer at a temperature of 50°C; after that the dissolved ammonium hydroxide solution (50 mL) was added slowly to control the agglomeration. The obtained cobalt hydroxide is calcined in air for 3 h at a temperature of 450°C yielding the  $\text{Co}_3\text{O}_4$  nanoparticles. The TEM image of the synthesized  $\text{Co}_3\text{O}_4$  nanoparticles is shown in **Figure 1**. Salavati-Niasari et al. [13] prepared  $\text{Co}_3\text{O}_4$  nanoparticles from a solid organometallic molecular precursor of N,N'-bis(salicylaldehyde)-1,2-phenylenediamino cobalt(II); Co(salophen) estimated the magnetic behavior of the  $\text{Co}_3\text{O}_4$  nanoparticles. In another study, Salavati-Niasari et al. [14] used thermal deposition method for the preparation of

Co<sub>3</sub>O<sub>4</sub> nanoparticles by using benzene dicarboxylate complexes, especially phthalate ones, as precursors and characterized using Fourier transform infrared and X-ray photoelectron spectroscopy and observed temperature-dependent

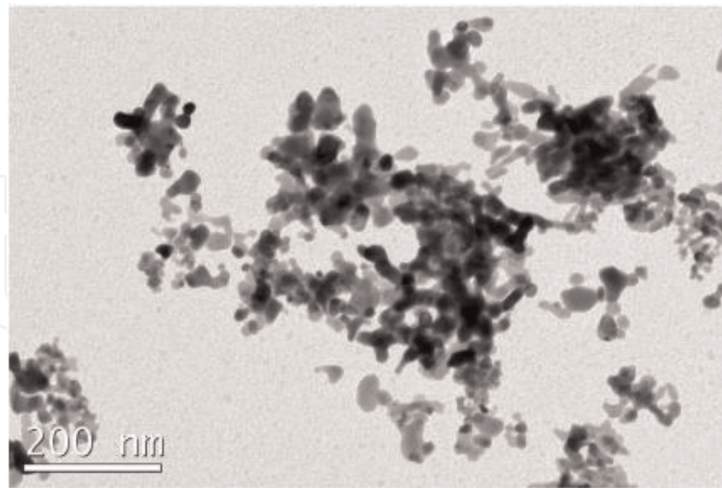


**Figure 1.**  
TEM image of synthesized Co<sub>3</sub>O<sub>4</sub> nanoparticles [12].

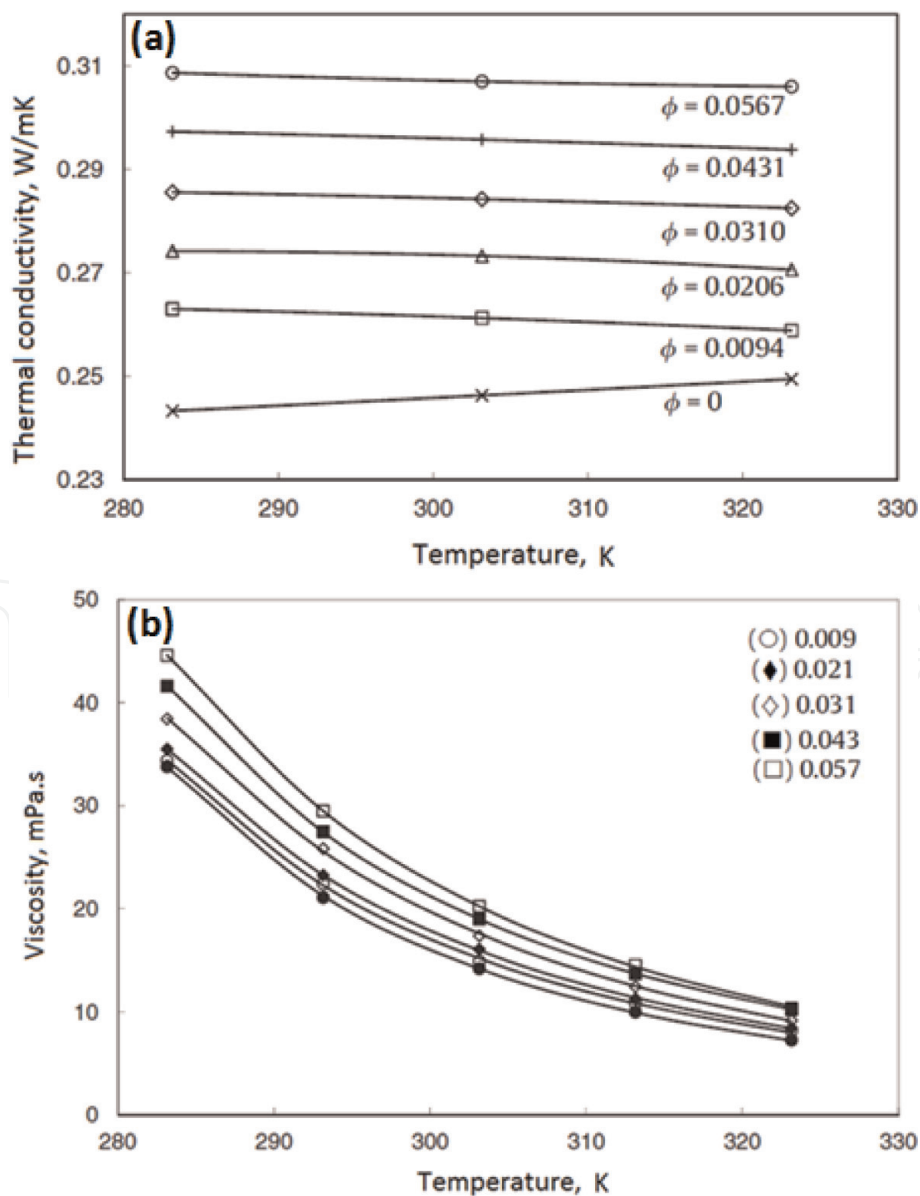


**Figure 2.**  
Co<sub>3</sub>O<sub>4</sub> nanofluids: (a) thermal conductivity and (b) viscosity [12].

magnetization curve in zero-field-cooled, where  $\text{Co}_3\text{O}_4$  nanoparticles exhibit weak ferromagnetism. Alrehaily et al. [15] synthesized  $\text{Co}_3\text{O}_4$  nanoparticles by gamma irradiation of 0.2–0.3 mM of  $\text{CoSO}_4$  solutions. Syam Sundar et al. [18] used chemical coprecipitation method for the synthesis of  $\text{Co}_3\text{O}_4$  nanoparticles, and they estimated their thermal properties at different particle volume concentrations and temperatures.

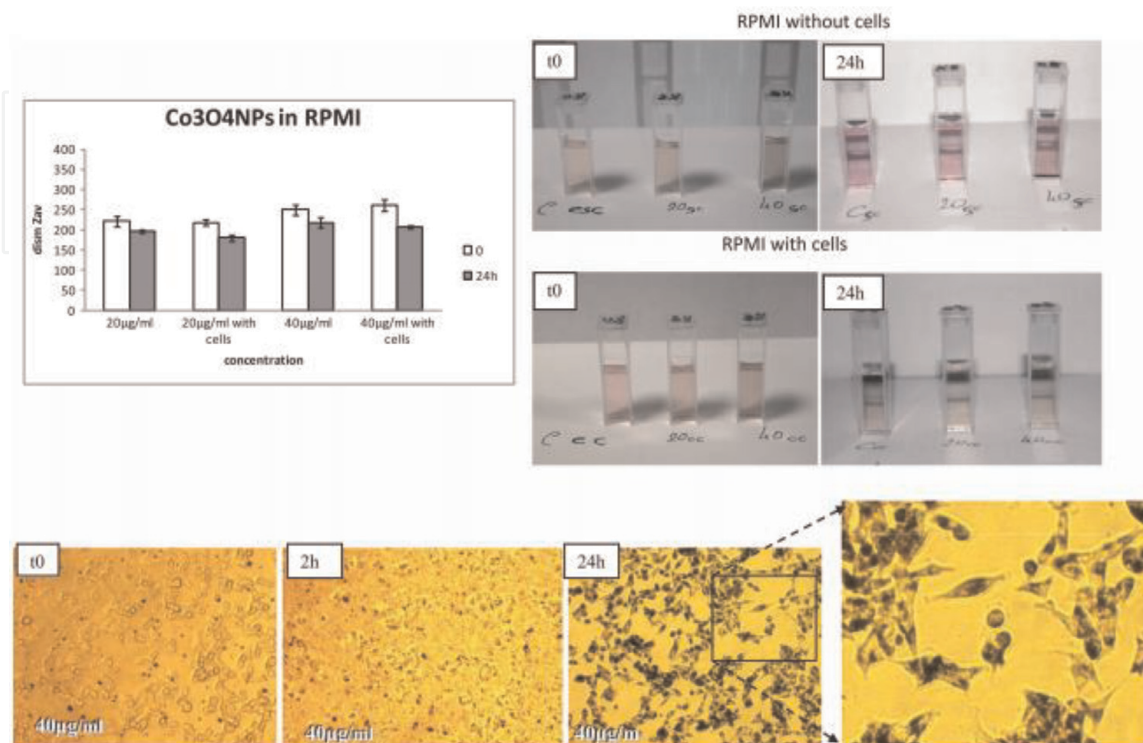


**Figure 3.**  $\text{Co}_3\text{O}_4$  nanoparticle toxicity in A549 cells: hydrodynamic size distributions of  $\text{Co}_3\text{O}_4$  nanoparticles in RPMI 1640 medium with 10% fetal bovine serum (FBS) at  $t = 0$  and after a 24-h exposure without and with A549 cells. In the right panels, the relative  $\text{Co}_3\text{O}_4$  NP suspensions used for DLS measurements, showing NP sedimentation after a 24-h exposure in the medium without cells [16].

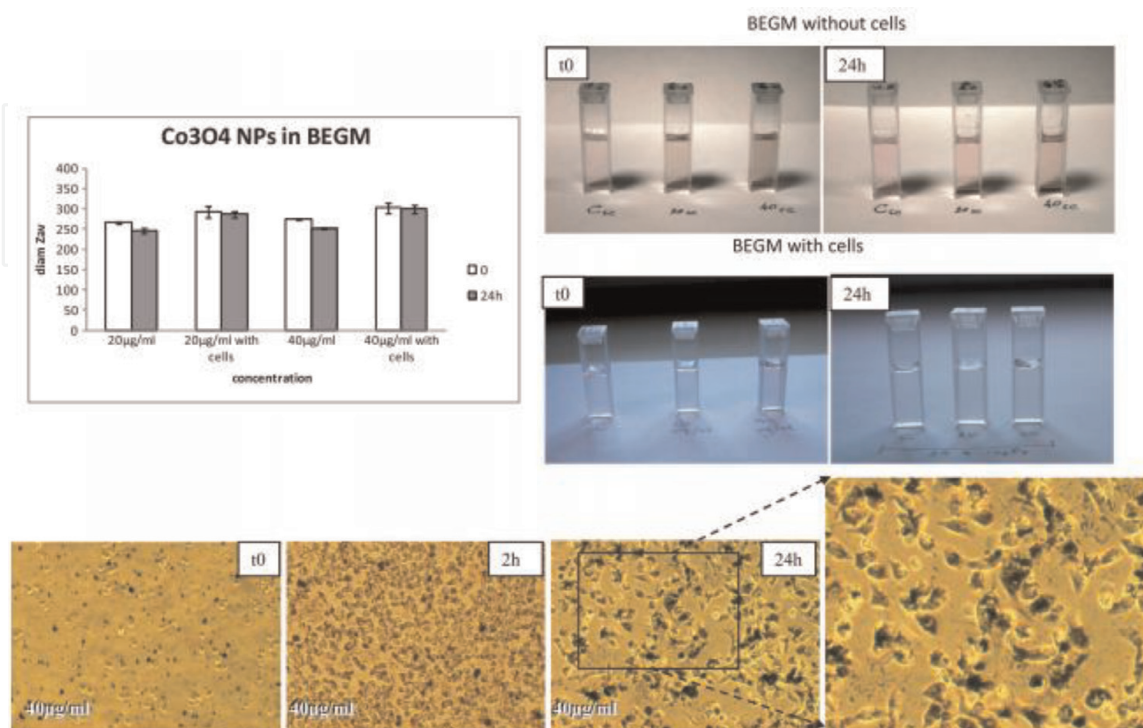


**Figure 4.**  $\text{Co}_3\text{O}_4$  nanoparticle toxicity in BEAS-2B cells: hydrodynamic size distribution of  $\text{Co}_3\text{O}_4$  nanoparticles in BEGM medium at  $t = 0$  and after a 24-h exposure without and with BEAS-2B cells [16].

## 2.2 Thermal properties

$\text{Co}_3\text{O}_4$  nanofluids have a potential use in several mechanical engineering applications; in particular, as replacement of low thermal conductivity fluids such as water and ethylene glycol, as a consequence, the thermal properties of nanofluids are of great interest. Mariano et al. [12] prepared  $\text{Co}_3\text{O}_4$  nanofluids by dispersing cobalt(II, III) oxide nanopowder in ethylene glycol and determined experimentally their thermal conductivity and viscosity. The thermal conductivity and viscosity of  $\text{Co}_3\text{O}_4/\text{EG}$  nanofluids are shown in **Figure 2a** and **b**; it is noticed that the increase of particle volume concentration ( $\phi$ ) yields increased values of thermal conductivity and viscosity. They observed thermal conductivity enhancement for 5.7% volume concentration of  $\text{Co}_3\text{O}_4/\text{EG}$  nanofluids is 27% at temperature of 323.15 K (**Figure 2a**); similarly, the viscosity enhancement for 5.7% volume concentration of  $\text{Co}_3\text{O}_4/\text{EG}$  nanofluids is 40% at a temperature of 303.15 K (**Figure 2b**).

## 2.3 Toxicity

Knowledge about the toxicity of  $\text{Co}_3\text{O}_4$  nanoparticles is very important considering their eventual use in medical applications. Cavallo et al. [16] studied the cytotoxicity of  $\text{Co}_3\text{O}_4$  nanoparticles in human alveolar (A549) and bronchial

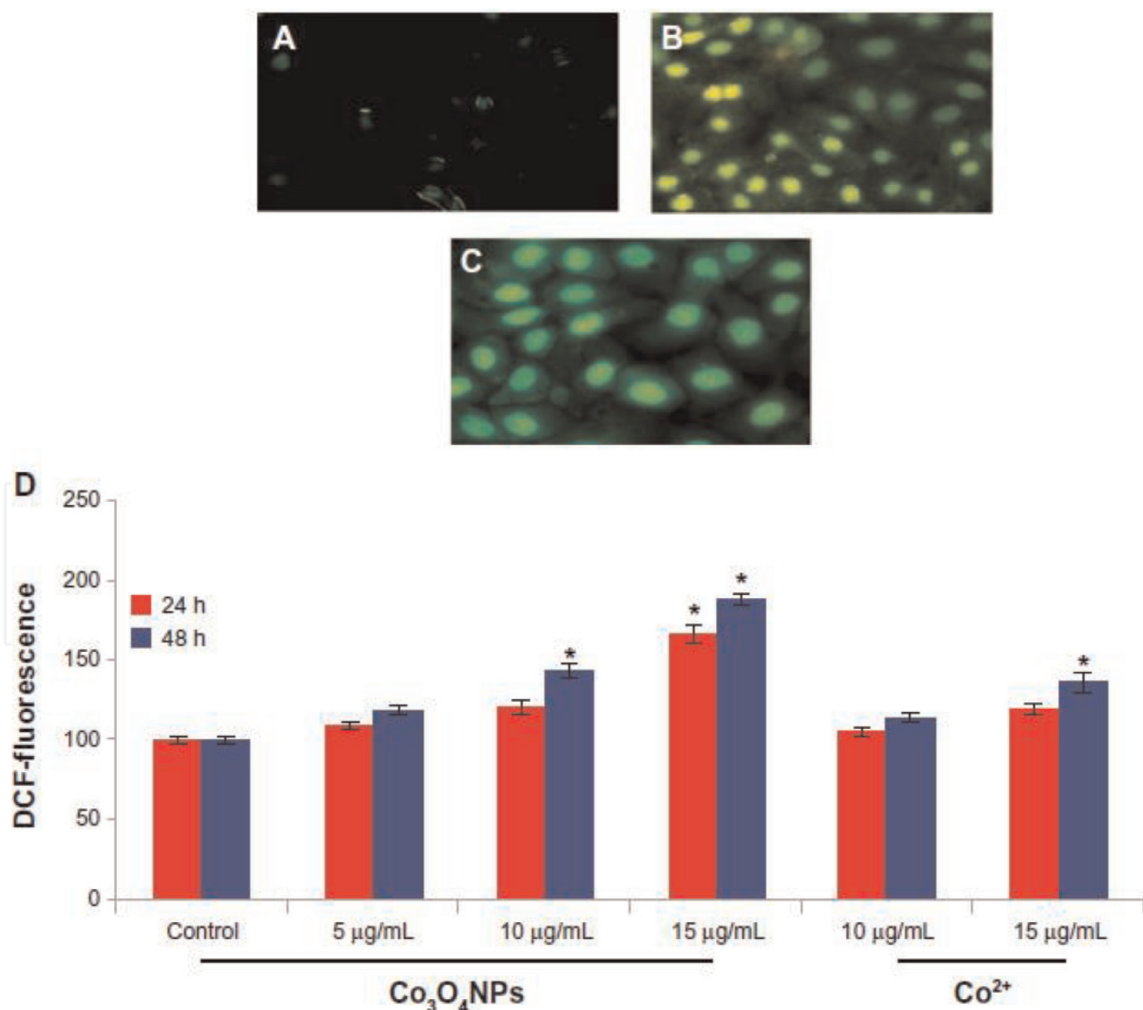


**Figure 5.**  $\text{Co}_3\text{O}_4$  nanoparticle toxicity in HepG2 cells: representative microphotographs showing  $\text{Co}_3\text{O}_4$  NP- and  $\text{Co}^{2+}$ -induced ROS generation in HepG2 cells. Images were snapped with Nikon phase contrast with a fluorescence microscope. (A) Control, (B) 15 µg/mL of  $\text{Co}^{2+}$ , (C) 15 µg/mL of  $\text{Co}_3\text{O}_4$  NPs, and (D) percentage change in ROS generation after 24 and 48 h of exposure to various concentrations of  $\text{Co}_3\text{O}_4$  NPs and  $\text{Co}^{2+}$  in HepG2 cells [17].

(BEAS-2B) cells exposed to 1 – 40  $\mu\text{g}/\text{mL}$ . In A549 cells, they found no cytotoxicity; however, BEAS-2B cells presented viability reduction at 40  $\mu\text{g}/\text{mL}$  and early membrane damage at 1, 5, and 40  $\mu\text{g}/\text{mL}$ . The results related to toxicity study are presented in **Figures 3** and **4**. Alarifi et al. [17] investigated the toxicity of  $\text{Co}_3\text{O}_4$  nanoparticles in HepG2 cells and observed cytotoxicity and genotoxicity in HepG2 cells through ROS and oxidative stress, and their results are presented in **Figure 5**.

### 3. Graphene oxide (GO)/cobalt oxide ( $\text{Co}_3\text{O}_4$ ) nanoparticles

#### 3.1 Synthesis procedure

The GO/ $\text{Co}_3\text{O}_4$  composite nanoparticles were synthesized and used for various applications. Liang et al. [22] synthesized  $\text{Co}_3\text{O}_4/\text{N}$ -doped graphene hybrid nanoparticles as catalyst for oxygen reduction. They prepared GO sheet using the modified Hummers method; after the  $\text{Co}_3\text{O}_4/\text{rmGO}$  hybrid was synthesized using a  $\text{Co}(\text{OAc})_2$  aqueous solution dispersed in GO/ethanol at room temperature and stirred for 10 h at a temperature of  $80^\circ\text{C}$ , then  $\text{NH}_4\text{OH}$  was added to the solution. They used the GO/ $\text{Co}_3\text{O}_4$  composite nanoparticles for catalytic activity. Syam Sundar et al. [18] synthesized the GO/ $\text{Co}_3\text{O}_4$  hybrid nanoparticles using the chemical coprecipitation method. Their procedure involved first the preparation of GO sheets using modified Hummers method, after that, 0.2 g of GO-COOH nanosheet dispersed in 100 mL of distilled water and added the solution to 0.4 g of  $\text{CoCl}_2 \cdot 6\text{H}_2\text{O}$  dispersed in 20 mL of distilled water and added 0.2932 g of  $\text{NaBH}_4$ , which was accompanied by the formation of a black precipitate. They prepared GO/ $\text{Co}_3\text{O}_4$  hybrid nanofluids and observed higher values of thermal conductivity and viscosity when particle concentration and temperature increase. The synthesis method and TEM results are shown in **Figure 6**. The XRD, FTIR, and VSM results are presented in **Figure 7a–c**. The XRD patterns of GO/ $\text{Co}_3\text{O}_4$  nanoparticles contain

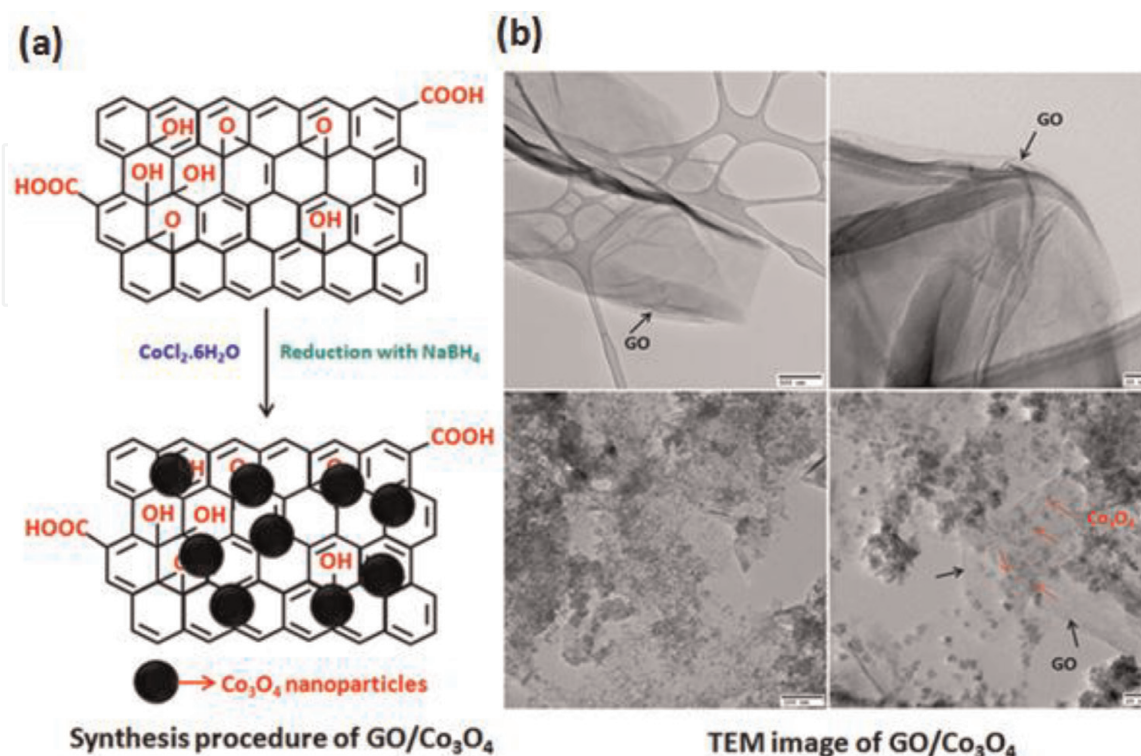


**Figure 6.** GO/ $\text{Co}_3\text{O}_4$  nanoparticles: (a) synthesis method and (b) TEM image [18].

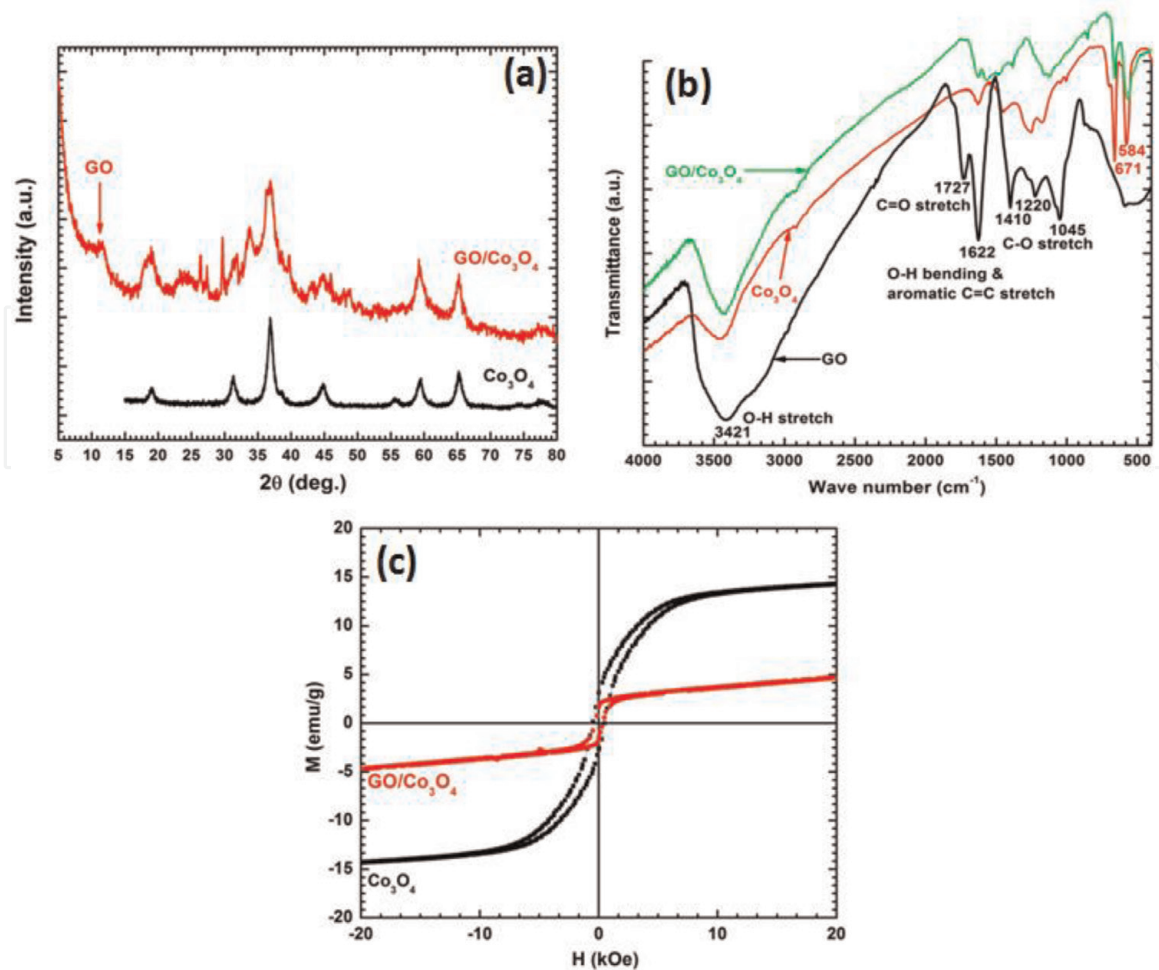


**Figure 7.** GO/Co<sub>3</sub>O<sub>4</sub> nanoparticles: (a) XRD patterns, (b) FTIR spectra, and (c) M-H curves [18].

both the peaks of Co<sub>3</sub>O<sub>4</sub> and GO. The 2θ position of GO/Co<sub>3</sub>O<sub>4</sub> nanoparticles is 11.68, 19.2, 31.2, 36.9, 44.8, 55.43, 59.4, and 65.2° which can be indexed as (002) plane for GO and (111), (220), (311), (400), (511), and (440) planes for Co<sub>3</sub>O<sub>4</sub> nanoparticles (Figure 7a). The IR spectra of GO nanoparticle (Figure 7c) show the GO peak at 1622 cm<sup>-1</sup> is the aromatic C=C group, the peak at 1727 cm<sup>-1</sup> is the C=O vibration of carboxylic group, and the peaks at 1045 cm<sup>-1</sup>, 1220 cm<sup>-1</sup>, and 1410 cm<sup>-1</sup> are contributed to C—O—C vibration of epoxy or alkoxy group. The IR spectra of Co<sub>3</sub>O<sub>4</sub> nanoparticle show the strong band peak at 584 cm<sup>-1</sup> and 671 cm<sup>-1</sup> is due to the Co—O vibration of Co<sub>3</sub>O<sub>4</sub> nanoparticles, which shows that Co<sup>2+</sup> has been oxidized into Co<sub>3</sub>O<sub>4</sub> nanoparticles. The IR spectra of GO/Co<sub>3</sub>O<sub>4</sub> nanoparticles show the peaks at 1622, 1727, 1045, 1220, and 1410 cm<sup>-1</sup> reflect C=C, C=O, and C—O—C groups related to GO and the peaks at 584 and 671 cm<sup>-1</sup> reflect the Co—O groups related to Co<sub>3</sub>O<sub>4</sub> nanoparticles. The total saturation magnetization of GO/Co<sub>3</sub>O<sub>4</sub> (Figure 7c) is 4.67 emu/g and pure Co<sub>3</sub>O<sub>4</sub> nanoparticles is 14.23 emu/g. The weight percentages of GO and Co<sub>3</sub>O<sub>4</sub> nanoparticles present in the GO/Co<sub>3</sub>O<sub>4</sub> nanocomposite particles were 67 and 33%, respectively. Shi et al. [20] prepared different concentrations of Co<sub>3</sub>O<sub>4</sub>/GO such as 20% Co<sub>3</sub>O<sub>4</sub>/GO, 30% Co<sub>3</sub>O<sub>4</sub>/GO, 50% Co<sub>3</sub>O<sub>4</sub>/GO, 70% Co<sub>3</sub>O<sub>4</sub>/GO, 90% Co<sub>3</sub>O<sub>4</sub>/GO, 95% Co<sub>3</sub>O<sub>4</sub>/GO, and pure Co<sub>3</sub>O<sub>4</sub>, and they studied their catalyst activity; the highest catalytic activity was observed when the Co<sub>3</sub>O<sub>4</sub> loading was about 50% in the catalyst. Xiang et al. [21] synthesized 20-nm-sized Co<sub>3</sub>O<sub>4</sub> nanoparticles, which were in situ grown on the chemically reduced graphene oxide (rGO) sheets to form an rGO/Co<sub>3</sub>O<sub>4</sub> composite during hydrothermal processing; they were used as the pseudocapacitor electrode in the



2 M KOH aqueous electrolyte solution, and the measured specific capacitance was 472 F/g at a scan rate of 2 mV/s.

### 3.2 Thermal properties

The water- and ethylene glycol-based GO/Co<sub>3</sub>O<sub>4</sub> nanocomposite nanofluid's thermal properties were measured by Syam Sundar et al. [18], and the results are shown in **Figures 8** and **9** at different volume concentrations and temperatures. It is noticed that the thermal conductivity of nanofluids increases linearly with the increase of particle volume concentrations and temperatures. Similarly, the viscosity of nanofluids increases with an increase of particle volume concentrations and decreases with an increase of temperature. The thermal conductivity of 0.05% nanofluid is enhanced by 2.82% and 8.58% at temperatures of 20 and 60°C, respectively, as compared to water. The thermal conductivity of 0.2% nanofluid is enhanced by 7.64 and 19.14% at temperatures of 20 and 60°C, respectively, as compared to water (**Figure 8**, left side). The viscosity of 0.05% volume concentration of nanofluid is enhanced by 1.075 times and 1.166 times; the viscosity of 0.2% volume concentration of nanofluid is enhanced by 1.49 times and 1.70 times at temperatures of 20 and 60°C compared to water (**Figure 8**, right side).

The thermal conductivity of 0.05% nanofluid is enhanced by 2.71 and 4.44% at temperatures of 20 and 60°C, respectively, as compared to EG. The thermal conductivity of 0.2% nanofluid is enhanced by 5.81 and 11.85% at temperatures of 20 and 60°C, respectively, as compared to EG (**Figure 9**, left side). The viscosity enhancement of 0.05% volume concentration of nanofluid is 1.028 times and 1.096 times; the viscosity enhancement of 0.2% volume concentration of nanofluid is 1.22 times and 1.42 times at temperatures of 20 and 60°C compared to EG (**Figure 9**, right side).

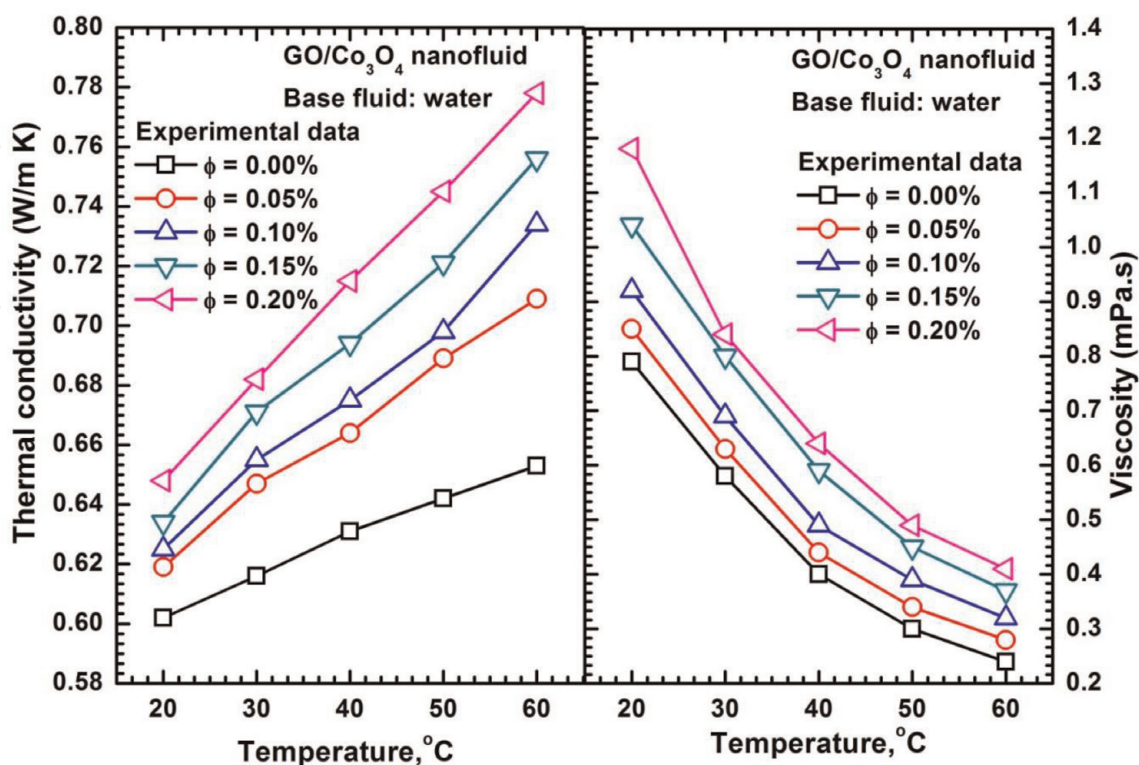


**Figure 8.** Water-based GO/Co<sub>3</sub>O<sub>4</sub> nanofluids: thermal conductivity (left side) and viscosity (right side) [18].

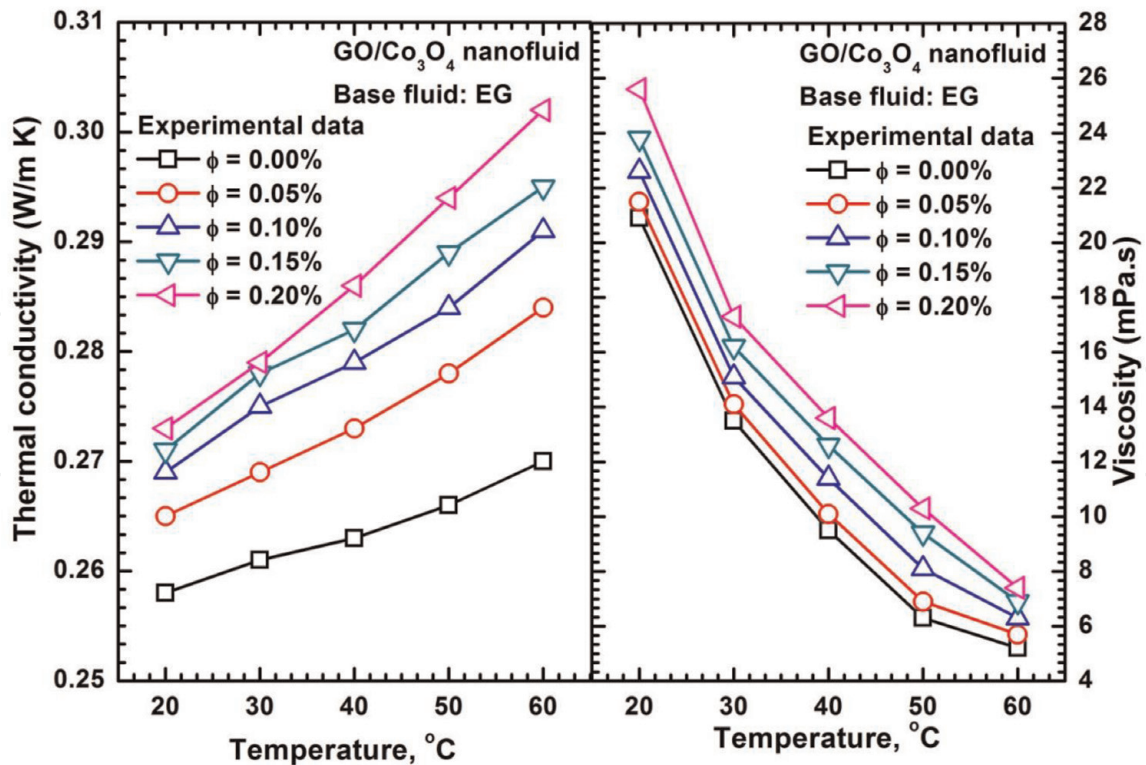


**Figure 9.** Ethylene glycol-based  $\text{GO}/\text{Co}_3\text{O}_4$  nanofluids: thermal conductivity (left side) and viscosity (right side) [18].

### 3.3 Electrical properties

Xiang et al. [21] measured the electrical properties of  $\text{GO}/\text{Co}_3\text{O}_4$  using pseudocapacitor electrode in 2 M of KOH aqueous electrolyte solution. **Figure 10** depicts the galvanostatic charge discharge curve of rGO and the  $\text{rGO}/\text{Co}_3\text{O}_4$  composite electrodes between 0 and 0.85 V at different current densities. Both the samples of rGO and  $\text{rGO}/\text{Co}_3\text{O}_4$  electrodes exhibited good symmetric shape with the coulomb efficiency close to 1. The  $\text{rGO}/\text{Co}_3\text{O}_4$  composite electrode presented longer charge discharge time than the rGO electrode, indicating larger specific capacitance (**Figure 10a** and **b**). The specific capacitance of the  $\text{rGO}/\text{Co}_3\text{O}_4$  electrode was investigated with a progressively increasing current density (**Figure 10c**). The specific capacitance decreases from 458 to 416 F/g with an increase in the current density from 0.5 to 2.0 A/g, respectively. The long-term stability of the  $\text{rGO}/\text{Co}_3\text{O}_4$  electrode was observed at the current density of 2.0 A/g. The specific capacitance of the  $\text{rGO}/\text{Co}_3\text{O}_4$  electrode increased during the first 100 cycles, which was due to an activation process in the super capacitor electrode. About 95.6% of the specific capacitance of  $\text{rGO}/\text{Co}_3\text{O}_4$  electrode was retained at the current density of 2.0 A/g after 1000 cycles (**Figure 10d**), which demonstrated its high cycling stability. Lai et al. [23] synthesized  $\text{Co}_3\text{O}_4$  nanoparticles grown on nitrogen-modified microwave-exfoliated graphite oxide (NMEG) with weight ratio controlled from 10 to 70%; due to their electrochemical performance, they are used as Li-ion battery anode, and they exhibit improved cycle stability. Seventy percent of the  $\text{Co}_3\text{O}_4/\text{NMEG}$  composite has an initial irreversible capacity of 230 mAh/g (first cycle efficiency of 77%), and 910 mAh/g of capacity is retained after 100 cycles. Seventy percent of  $\text{Co}_3\text{O}_4/\text{tRG-O}$  delivers a reversible capacity of 750 mAh/g, and the irreversible capacity loss during the first cycle is 700 mAh/g. It is noted that the composite material synthesized with  $\text{Co}_3\text{O}_4$  exhibits larger specific capacitance than rGO material when they are used as electrode. The  $\text{Co}_3\text{O}_4/\text{NMEG}$  composite material shows higher capacitance when they are used as Li-ion battery

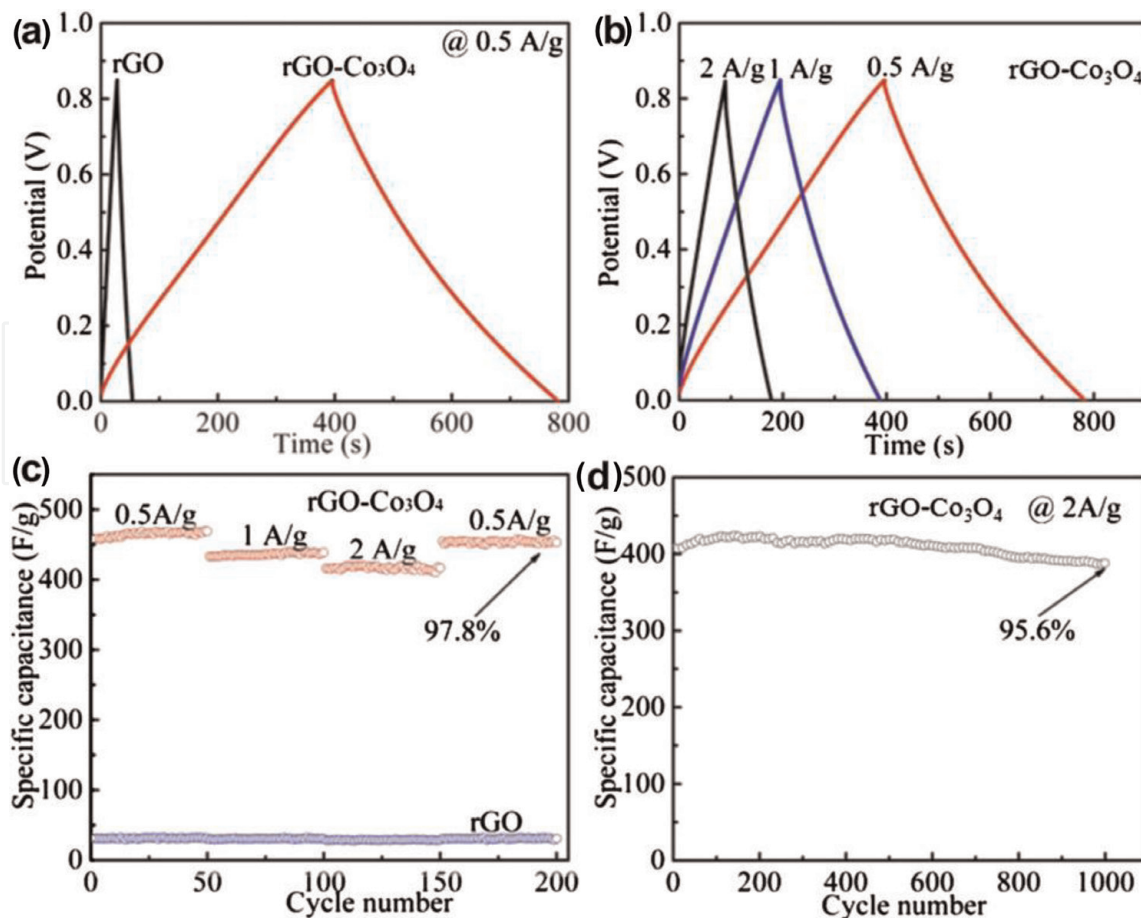


**Figure 10.** *GO/Co<sub>3</sub>O<sub>4</sub> nanomaterial: (a) charge-discharge curves at the current density of 0.5 A/g, (b) charge-discharge curves at different current densities (0.5, 1.0, and 2.0 A/g), (c) cycling stability at varying the current density, and (d) long-term stability at a current density of 2.0 A/g [21].*

anode. So, it is understood that the composite material exhibits synergistic (superior electrical) properties compared to the single-phase nanoparticles.

## 4. Nanodiamond (ND)-cobalt oxide (Co<sub>3</sub>O<sub>4</sub>) nanoparticles

### 4.1 Synthesis procedure

The ND-Co<sub>3</sub>O<sub>4</sub> nanoparticles were synthesized by Syam Sundar et al. [19] using in situ and the chemical coprecipitation method. The synthesis route and TEM results are shown in **Figure 11**. The synthesis route contains dispersion of 0.5 g of ND particles and 0.5 g (0.003 M) of CoCl<sub>2</sub>·6H<sub>2</sub>O in 100 mL, adds 0.379 (0.01 M) g of NaBH<sub>4</sub> gradually, and observes the formation of light black color precipitate. The XRD, VSM, and XPS results of ND-Co<sub>3</sub>O<sub>4</sub> nanocomposite are reported in **Figure 10**.

The XRD, VSM, and prepared nanofluids are shown in **Figure 12a–d**. From the XRD patterns (**Figure 12a**), the 2θ position for the ND nanoparticles for the plane (111) is 43.73°; similarly, the 2θ position for the Co<sub>3</sub>O<sub>4</sub> nanoparticles for the plane (311) is 36.81°, and the ND-Co<sub>3</sub>O<sub>4</sub> nanocomposite nanoparticles contains both the ND and Co<sub>3</sub>O<sub>4</sub> nanoparticles planes. The weight percentage of ND and Co<sub>3</sub>O<sub>4</sub> present in the ND-Co<sub>3</sub>O<sub>4</sub> nanocomposite was measured from vibrating sample magnetometer (Cryogenic, UK) instrument (**Figure 12b**). The total saturation magnetization of Co<sub>3</sub>O<sub>4</sub> nanoparticles is 14.3 emu/g, whereas the total saturation magnetization of ND-Co<sub>3</sub>O<sub>4</sub> nanocomposite is 4.7 emu/g. It is decreased

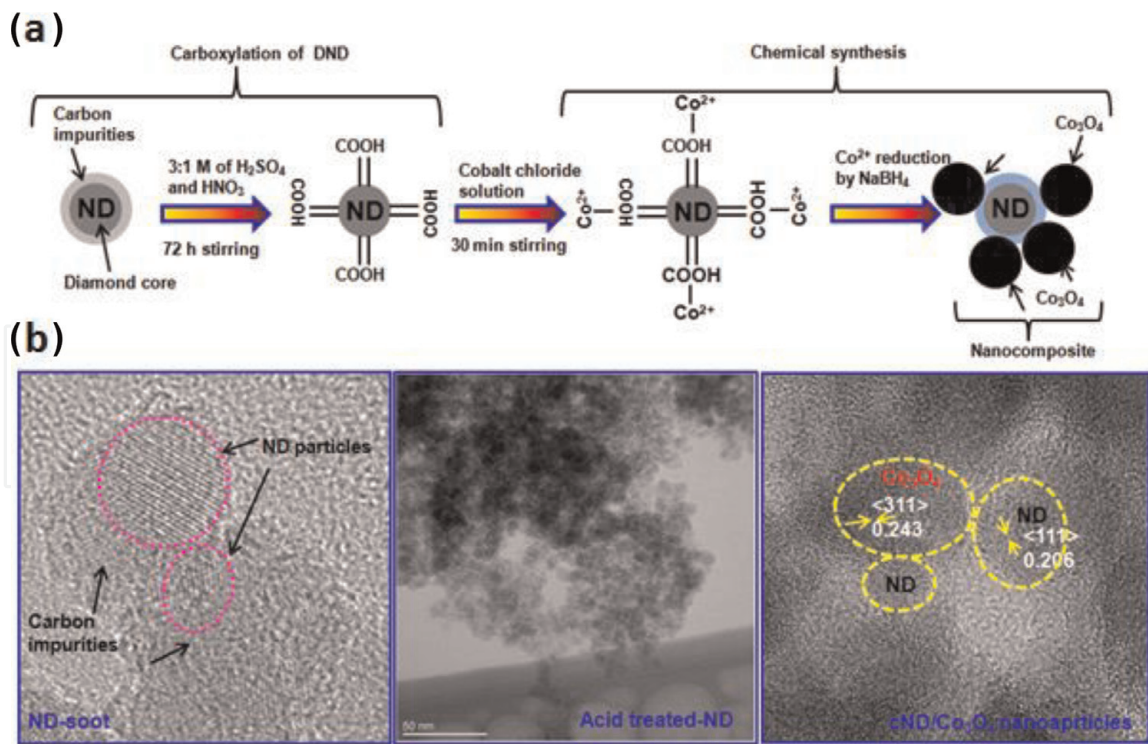


**Figure 11.** ND- $\text{Co}_3\text{O}_4$  nanoparticles: (a) synthesized method and (b) TEM image [19].

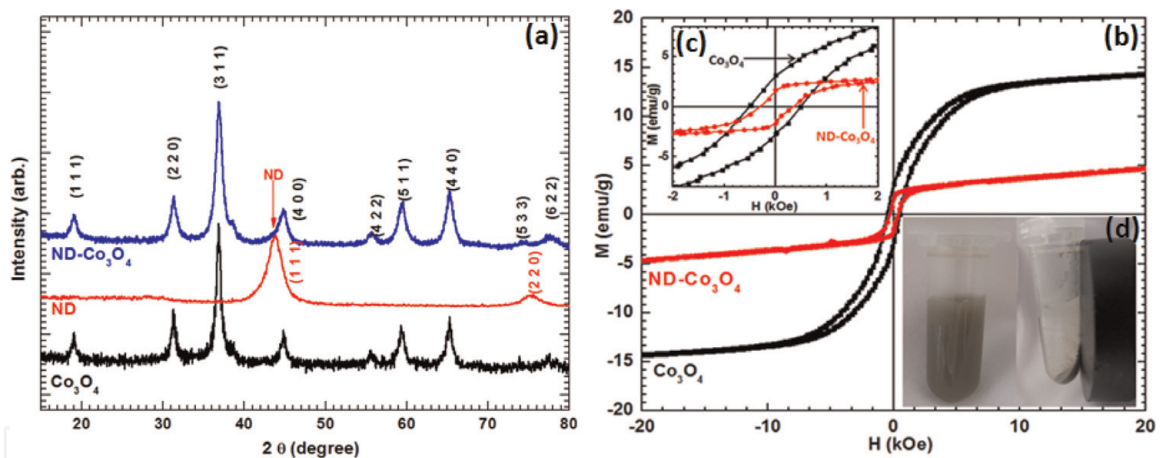


**Figure 12.** ND- $\text{Co}_3\text{O}_4$  nanoparticles: (a) XRD patterns, (b)  $M$ - $H$  curve, (c) coercivity, and (d) the ND- $\text{Co}_3\text{O}_4$  nanofluids [19].

because of the presence of nonmagnetic material of ND. The coercivity results of ND- $\text{Co}_3\text{O}_4$  and of pure  $\text{Co}_3\text{O}_4$  nanoparticles are 334 and 490 Oe, respectively (Figure 12c). Based on the total sum rule, it is observed that there is 67% of ND and 33% of  $\text{Co}_3\text{O}_4$  present in the ND- $\text{Co}_3\text{O}_4$  nanocomposite nanoparticles. The prepared ND- $\text{Co}_3\text{O}_4$  nanofluid's samples are shown in Figure 12d, and the final ND- $\text{Co}_3\text{O}_4$  nanocomposite particles showing magnetic behavior are observed.

The surface composition of ND- $\text{Co}_3\text{O}_4$  nanocomposite particles was measured using X-ray photoelectron spectroscopy (XPS), and the results are shown in Figure 13a–c. The Co 2p spectra has two main peaks at binding energies (BEs) of 780.7 and 796.3 eV, which can be related to Co 2p<sub>3/2</sub> and Co 2p<sub>1/2</sub> spin-orbit lines, respectively (Figure 13a). The determination of oxidation state of the each and every component is very important, and also it is very difficult. The shape of the satellites and the energy gap between the satellites are the key parameters used to discriminate between different oxidation states of Co. For instance, the presence of

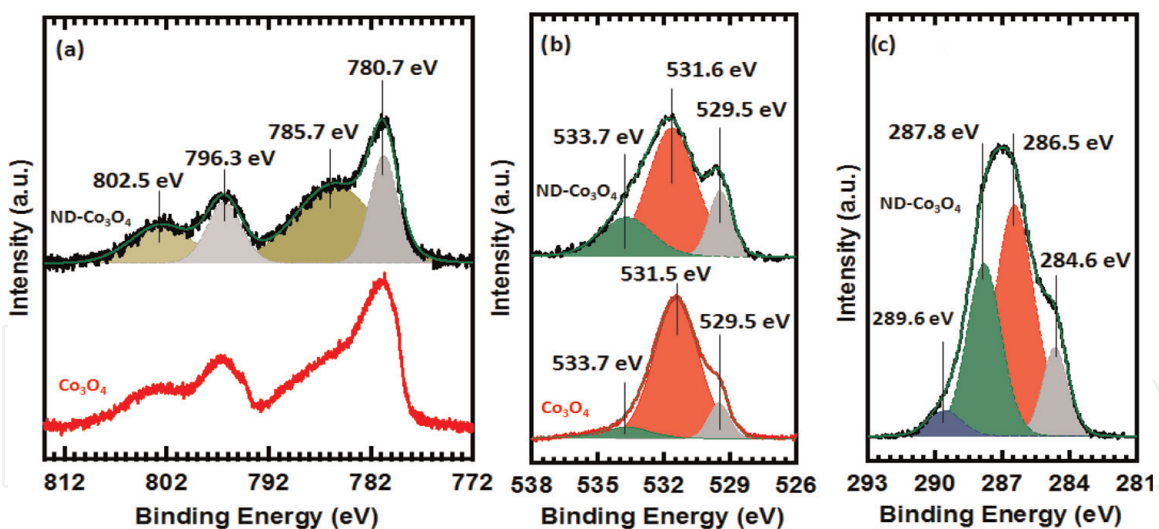


**Figure 13.** ND- $\text{Co}_3\text{O}_4$  nanocomposite—XPS spectra: (a) Co 2P, (b) O 1s, and (c) C 1s core levels [19].

a pronounced satellite like that founded in the present sample at 785.7 eV can be ascribed to CoO. For the case of  $\text{Co}_3\text{O}_4$  compounds, the satellite is generally detected at BEs higher than 10 eV with respect to the main peak. It is observed from the XPS analysis that the  $\text{Co}_3\text{O}_4$  particles are covered by a thin layer of CoO.

The O 1s core level is presented in **Figure 13b** for the cobalt nanoparticles (bottom) and for the nanocomposite (upper). The first component, centered at a BE = 529.5 eV (gray), is ascribed to oxygen atoms in the cobalt particles, while the others are related to different oxygen species. In particular, the components at 531.6 eV (red) and 533.7 eV (green) are ascribed to  $\text{OH}^-$  and  $\text{C}=\text{O}/\text{O}=\text{C}=\text{O}$ , respectively. Moreover, in the case of the nanocomposite, the C 1s core level (**Figure 13c**) shows interesting features. Four components were needed for fitting this peak, appearing at BEs of 284.6 eV (gray), 286.5 eV (red), 287.8 eV (green), and 289.6 eV (blue), which can be ascribed to  $\text{C}-\text{C}$ ,  $\text{C}-\text{OH}$  or  $\text{C}-\text{O}-\text{C}$ ,  $\text{C}=\text{O}$ , and  $\text{O}=\text{C}-\text{O}$ , respectively. Thus, XPS indicates that the cobalt particles are integrated with the treated nanodiamonds.

## 4.2 Thermal properties

The water- and ethylene glycol-based ND- $\text{Co}_3\text{O}_4$  nanofluid's thermal conductivity and viscosity were measured by Syam Sundar et al. [19], and the data is shown in **Figure 14a** and **b** at different particle weight concentrations and temperatures. The water-based ND- $\text{Co}_3\text{O}_4$  nanofluid's samples are shown in **Figure 14b**, and particle size distribution is shown in **Figure 14c**. They observed thermal conductivity enhancement of 2 and 6% for 0.05 wt.% of water-based ND- $\text{Co}_3\text{O}_4$  nanofluid and the thermal conductivity enhancement of 8.7 and 15.7% for 0.15 wt.% of water-based ND- $\text{Co}_3\text{O}_4$  nanofluid at temperatures of 20 and 60°C, respectively, compared with water data (**Figure 14a**). They also observed thermal conductivity enhancement of 1.16 and 3.97% for 0.05 wt.% of EG-based ND- $\text{Co}_3\text{O}_4$  nanofluid and the thermal conductivity enhancement of 4.68 and 8.71% for 0.15 wt.% of EG-based ND- $\text{Co}_3\text{O}_4$  nanofluid at temperatures of 20 and 60°C, respectively, compared with EG data (**Figure 14d**).

## 4.3 Toxicity of ND- $\text{Co}_3\text{O}_4$ nanoparticles

The toxicity of ND- $\text{Co}_3\text{O}_4$  nanoparticles was studied by Syam Sundar et al. [24] on *Allium cepa*, and the results are shown in **Figure 15**. The untreated root tip

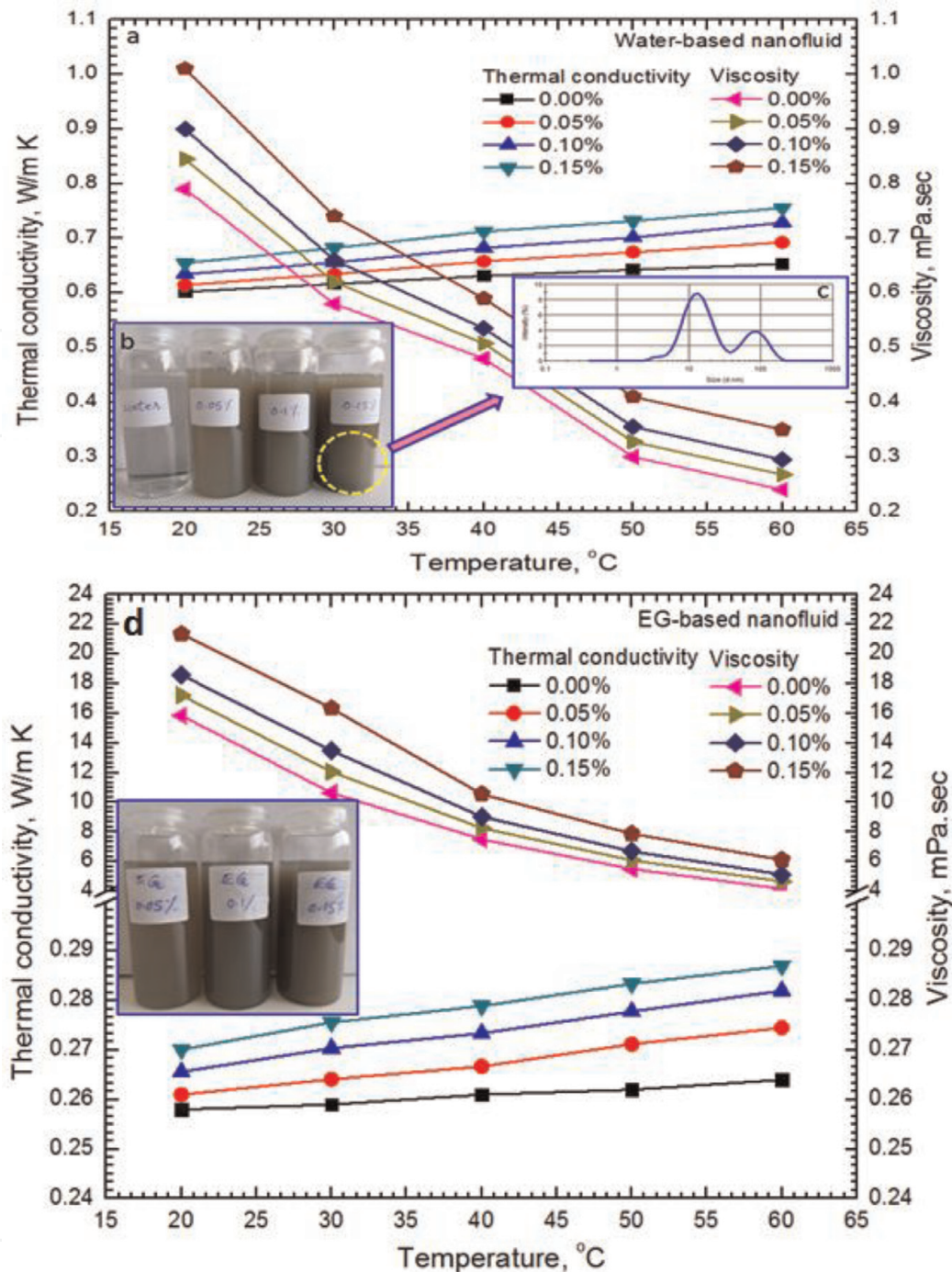


**Figure 14.** Thermal conductivity of ND-Co<sub>3</sub>O<sub>4</sub> nanofluids: (a) water-based nanofluids, (b) sample nanofluids, (c) particle size distribution, and (d) EG-based nanofluids [19].

cells showed a mitotic index of  $71.3 \pm 2.2\%$ . However, a dose-dependent effect on mitotic index was noted for Co<sub>3</sub>O<sub>4</sub> and Co<sub>3</sub>O<sub>4</sub>-cND. In particular, the mitotic indices were found to be  $58.07 \pm 1.7$ ,  $37.8 \pm 1.2$ , and  $28.6 \pm 0.8\%$  upon exposure to 5, 10, and 20  $\mu\text{g/mL}$  Co, respectively. Notably, decreases in MI were insignificant at these concentrations of cND with values of  $68.3 \pm 2.0$ ,  $65.7 \pm 1.9$ , and  $59.0 \pm 1.7$ , respectively. The ameliorative effect of Co-accrued impacts is demonstrated by low (5  $\mu\text{g/mL}$ ) and moderate (10  $\mu\text{g/mL}$ ) concentration values of cND-Co<sub>3</sub>O<sub>4</sub>. This indicates that, if accidentally released into the environment, cND-Co<sub>3</sub>O<sub>4</sub> would be safe for biotic life to a maximum concentration of 10  $\mu\text{g/mL}$ . The observed Co-accrued cyto-genotoxic consequences coincide with similar earlier studies, where Co oxide nanoparticles were reported to spoil the whole cellular metabolism and stages of cell division mainly by blocking water channels through

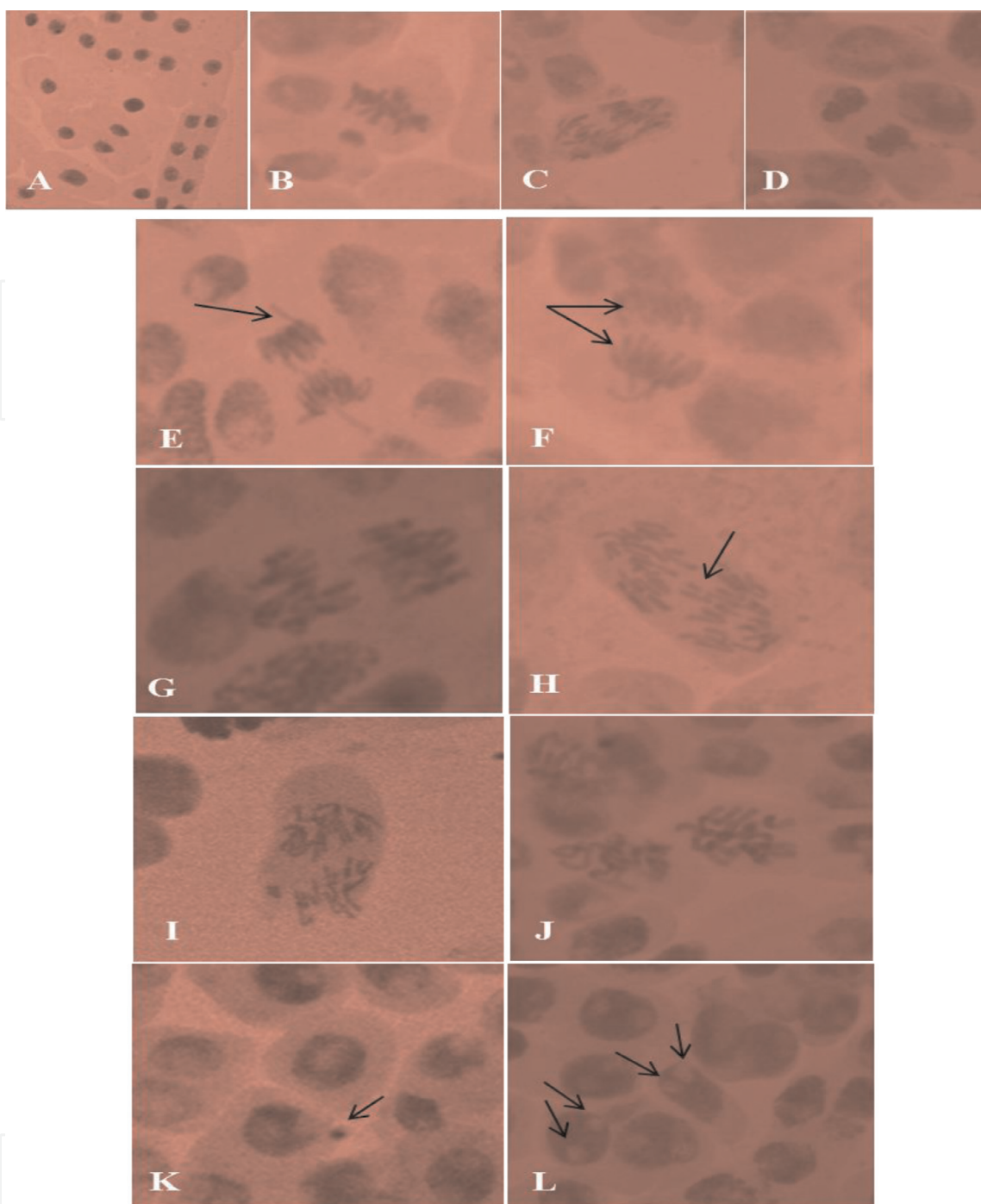


**Figure 15.** Toxicity tests on *Allium cepa* of ND- $\text{Co}_3\text{O}_4$  nanoparticles (A–D), various concentrations of cobalt oxide (E–G), and cND- $\text{Co}_3\text{O}_4$  (H–K). A = prophase, B = metaphase, C = anaphase, D = telophase, E = chromosomal break, F = cytoplasmic bridge, G = disturbed anaphase, H = laggard, I = sticky anaphase, J = scattered anaphase, K = prophase nuclei with micronucleus in interphase, L = binucleate cells [24].

adsorption and/or by impacting genetic material by causing various types of chromosomal aberrations.

In summary, insignificant changes in MI with moderate concentration (10  $\mu\text{g}/\text{mL}$ ) of cND- $\text{Co}_3\text{O}_4$  also confirm that cND- $\text{Co}_3\text{O}_4$  was unable to interfere with the normal development of mitosis mainly by its incapacity to prevent cells from entering the prophase and blocking the mitotic cycle during interphase inhibiting DNA/protein synthesis. Moreover, 20  $\mu\text{g}/\text{mL}$  of cND- $\text{Co}_3\text{O}_4$  compared to 5, 10, and 20  $\mu\text{g}/\text{mL}$  of  $\text{Co}_3\text{O}_4$  and 10  $\mu\text{g}/\text{mL}$  of cND- $\text{Co}_3\text{O}_4$  presents insignificant and infrequent chromosome aberrations (such as stickiness, breaks, disturbed, and scattered metaphase); therefore, these results strongly support the environment-friendly nature of the cND- $\text{Co}_3\text{O}_4$  nanocomposite, as demonstrated by the toxicity tests

conducted using *Allium cepa* (Figure 15A–D). For comparison purpose, similar tests are also performed for various concentrations of cobalt oxide nanoparticles (Figure 15E–G) and cND-Co<sub>3</sub>O<sub>4</sub> (H–K) (Figure 15H–K).

## 5. Zeolite Y/cobalt oxide (Co<sub>3</sub>O<sub>4</sub>) nanoparticles

### 5.1 Synthesis procedure

The zeolite Y/cobalt oxide (Co<sub>3</sub>O<sub>4</sub>) nanoparticles were synthesized by Davar et al. [25], and the schematic diagram is depicted in Figure 16. The Co<sub>3</sub>O<sub>4</sub> nanocomposite was synthesized by an ion exchange of cobalt ions and zeolite Y in the presence of sodium hydroxide and calcination treatment; the synthesized zeolite Y/Co<sub>3</sub>O<sub>4</sub> has a paramagnetic behavior at room temperature.

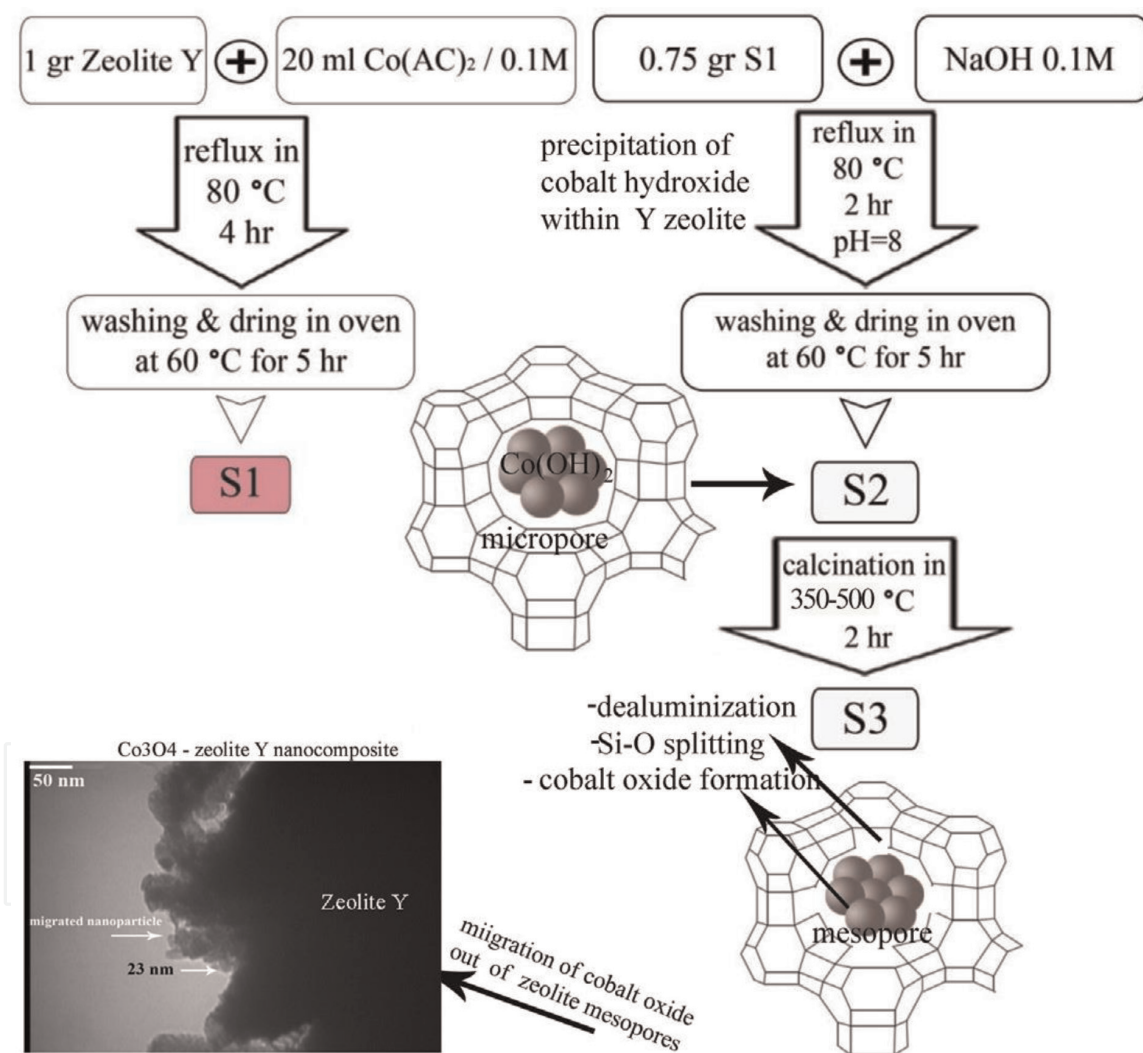


Figure 16.  
 Synthesis procedure of zeolite Y/Co<sub>3</sub>O<sub>4</sub> nanoparticles [25].

## 6. Carbon nanotubes/cobalt oxide (Co<sub>3</sub>O<sub>4</sub>) nanoparticles

### 6.1 Synthesis procedure

The f-SWCNT/Co<sub>3</sub>O<sub>4</sub> nanocomposite was prepared by Abdolmaleki et al. [26] using the electrostatic coprecipitation route. They noted that the specific



capacitance of f-SWCNT/ $\text{Co}_3\text{O}_4$  is high with a value of 343F/g, while that of the  $\text{Co}_3\text{O}_4$  nanoparticles is only 77F/g (**Figure 17**). Zarnegar et al. [27] used a new sonochemical synthesis of polyhydroquinolines having as catalyst  $\text{Co}_3\text{O}_4$ -CNT nanocomposites for aldehydes, dimedone, ethyl acetoacetate, and ammonium acetate in an ethanol medium. These nanocomposites proved to be a highly effective

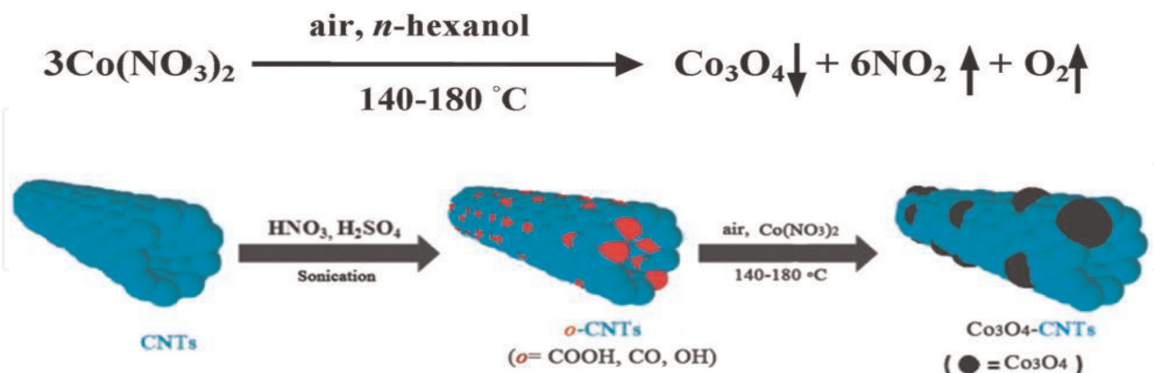


**Figure 17.**  
Synthesis procedure of MWCNT- $\text{Co}_3\text{O}_4$  nanoparticles [26].

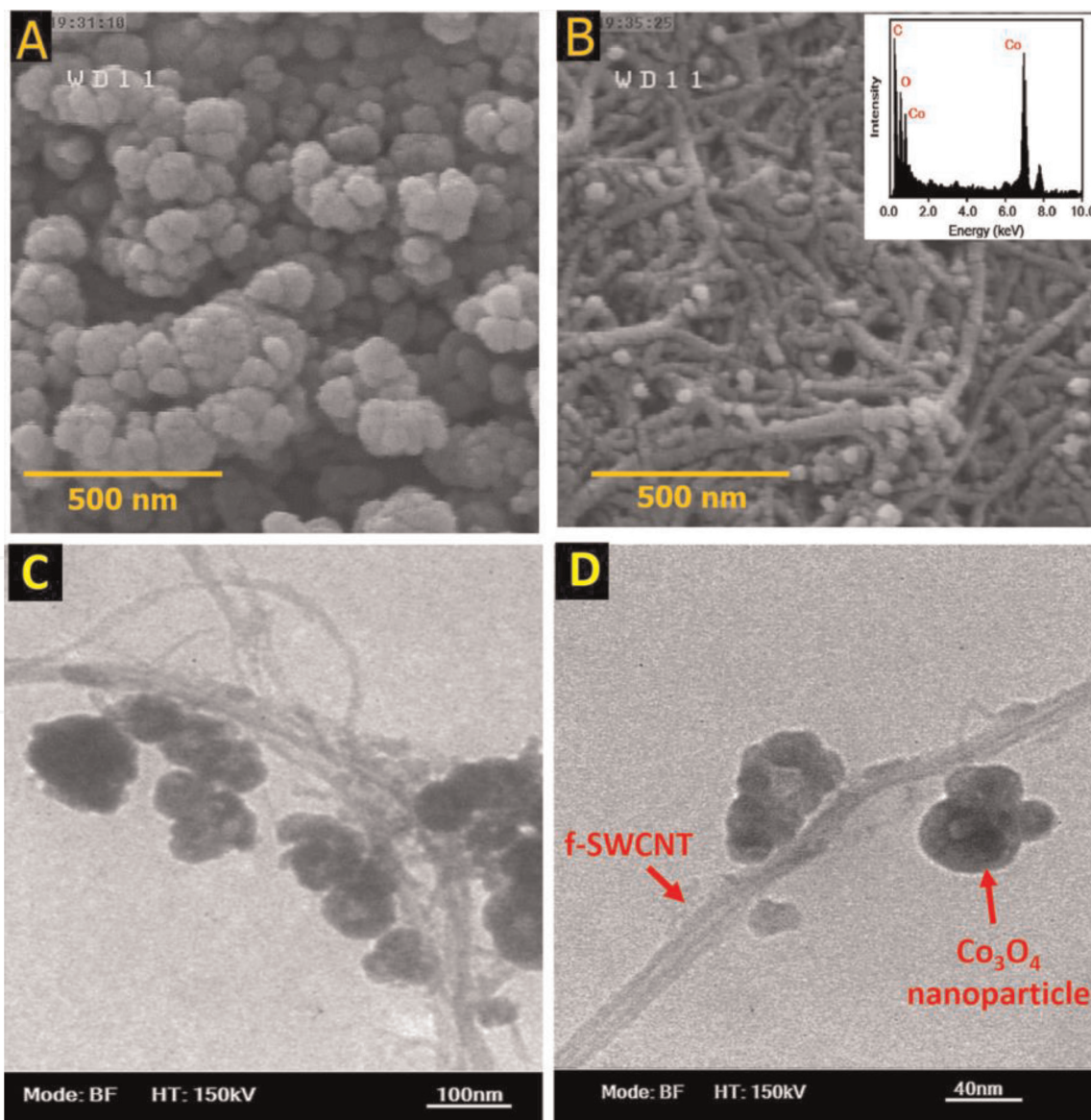


**Figure 18.**  
TEM results of MWCNT- $\text{Co}_3\text{O}_4$  nanoparticles [27], (a)  $\text{Co}_3\text{O}_4$ , (b) MWCNT, (c) MWCNT- $\text{Co}_3\text{O}_4$  nanoparticles at 100 nm range and (d) MWCNT- $\text{Co}_3\text{O}_4$  nanoparticles at 100 nm range.

catalytic system, and they provide a green strategy to generate a variety of polyhydroquinolines under sonic conditions. The TEM image of  $\text{Co}_3\text{O}_4$  nanoparticles (**Figure 18A**), carbon nanotubes (**Figure 18B**),  $\text{Co}_3\text{O}_4$ -CNT nanocomposites at microscope 100 nm range (**Figure 18C**), and  $\text{Co}_3\text{O}_4$ -CNT nanocomposites at microscope 40 nm range (**Figure 18D**) is shown in **Figure 18**.

## 7. Conclusions

The cobalt oxide-based composite nanoparticles and its engineering and medical applications were discussed in this book chapter. The pure  $\text{Co}_3\text{O}_4$  nanoparticles reveal the presence of toxicity, whereas cobalt compounds are nontoxic. In this book chapter, the synthesis procedure for cobalt and cobalt-based compounds such as  $\text{GO}/\text{Co}_3\text{O}_4$ ,  $\text{ND}-\text{Co}_3\text{O}_4$ , zeolite  $\text{Y}/\text{Co}_3\text{O}_4$ , and  $\text{MWCNT}-\text{Co}_3\text{O}_4$ . All the synthesized cobalt-based compound materials present magnetic properties, which can be benefit for the thermal applications, electrical applications, and medical applications. Cobalt oxide-based compounds have improved synergistic properties as compared to pure cobalt oxide nanoparticles.

## Acknowledgements

The author (LSS) acknowledges the Foundation for Science and Technology (FCT, Portugal) for the financial support received through the grant SFRH/BPD/100003/2014. The author (ACMS) acknowledges the 2017 Visiting Scientist Fellowship awarded to him under the Chinese Academy of Sciences President's International Fellowship Initiative. TEMA/DEM researchers also acknowledge the FCT grant UID/EMS/00481/2019-FCT, the infrastructures support CENTRO-01-0145-FEDER-022083-Centro Portugal Regional Operational Programme (Centro2020), and Project 33912-AAC no. 03/SI/2017, under the Portugal 2020 Partnership Agreement, through the European Regional Development Fund.

## Author details


Lingala Syam Sundar<sup>1\*</sup>, Manoj K. Singh<sup>1,2\*</sup>, António M.B. Pereira<sup>1</sup>  
and Antonio C.M. Sousa<sup>1</sup>

<sup>1</sup> Department of Mechanical Engineering, Centre for Mechanical Technology and Automation (TEMA-UA), University of Aveiro, Portugal

<sup>2</sup> Centre for Nano and Material Sciences, JAIN (Deemed-to-be University), Bengaluru, Karnataka, India

\*Address all correspondence to: [sslingala@gmail.com](mailto:sslingala@gmail.com) and [mksingh@ua.pt](mailto:mksingh@ua.pt)

## IntechOpen

© 2019 The Author(s). Licensee IntechOpen. This chapter is distributed under the terms of the Creative Commons Attribution License (<http://creativecommons.org/licenses/by/3.0>), which permits unrestricted use, distribution, and reproduction in any medium, provided the original work is properly cited. 

## References

- [1] Alinovi R, Goldoni M, Pinelli S, Campanini M, Aliatis I, Bersani D, et al. Oxidative and pro inflammatory effects of cobalt and titanium oxide nanoparticles on aortic and venous endothelial cells. *Toxicology In Vitro*. 2014;**29**:426-437
- [2] Cattaneo AG, Gornati R, Sabbioni E, Chiriva-Internati M, Cobos E, Jenkins MR, et al. Nanotechnology and human health: Risks and benefits. *Journal of Applied Toxicology*. 2010;**30**:730-744
- [3] Chattopadhyay S, Dash SK, Tripathy S, Das B, Mandal D, Pramanik P, et al. Toxicity of cobalt oxide nanoparticles to normal cells; an in vitro and in vivo study. *Chemico-Biological Interactions*. 2014;**226**:58-71
- [4] Cho WS, Duffin R, Bradley M, Megson IL, Macnee W, Howie SE, et al. NiO and Co<sub>3</sub>O<sub>4</sub> nanoparticles induce lung DTH-like responses and alveolar lipoproteinosis. *The European Respiratory Journal*. 2012;**39**:546-557
- [5] Cho WS, Duffin R, Bradley M, Megson IL, MacNee W, Lee JK, et al. Predictive value of in vitro assays depends on the mechanism of toxicity of metal oxide nanoparticles. *Particle and Fibre Toxicology*. 2013;**10**:55
- [6] Zhu Y, Stubbs LP, Ho F, Liu R, Ship CP, Maguire JA, et al. Magnetic nanocomposites: A new perspective in catalysis. *ChemCatChem*. 2010;**2**:365-374
- [7] Lim CW, Lee IS. Magnetically recyclable nanocatalyst systems for the organic reactions. *Nano Today*. 2010;**5**:412-434
- [8] Chen GJ, Wang LF. Design of magnetic nanoparticles-assisted drug delivery system. *Current Pharmaceutical Design*. 2011;**17**:2331-2351
- [9] Wan TJ, Shen SM, Siao SH, Huang CF, Cheng CY. Using magnetic seeds to improve the aggregation and precipitation of nanoparticles from backside grinding wastewater. *Water Research*. 2011;**45**:6301-6307
- [10] Yang HT, Su YK, Shen CM, Yang TZ, Goa HJ. Synthesis and magnetic properties of  $\epsilon$ -cobalt nanoparticles, *Surface and Interface Analysis*. 2004;**36**:155-160
- [11] Manigandan R, Giribabu K, Suresh R, Vijayalakshmi L, Stephen A, Narayanana V. Cobalt oxide nanoparticles: Characterization and its electrocatalytic activity towards nitrobenzene. *Chemical Science Transactions*. 2013;**2**(S1):S47-S50
- [12] Mariano A, Pastoriza-Gallego MJ, Lugo L, Mussari L, Piñeiro MM. Co<sub>3</sub>O<sub>4</sub> ethylene glycol-based nanofluids: Thermal conductivity, viscosity and high pressure density. *International Journal of Heat and Mass Transfer*. 2015;**85**:54-60
- [13] Salavati-Niasari M, Khansari A, Davar F. Synthesis and characterization of cobalt oxide nanoparticles by thermal treatment process. *Inorganica Chimica Acta*. 2009;**362**:4937-4942
- [14] Salavati-Niasari M, Mir N, Davar F. Synthesis and characterization of Co<sub>3</sub>O<sub>4</sub> nanorods by thermal decomposition of cobalt oxalate. *Journal of Physics and Chemistry of Solids*. 2009;**70**:847-852
- [15] Alrehaily LM, Joseph JM, Biesinger MC, Guzonas DA, Wren JC. Gamma-radiolysis-assisted cobalt oxide nanoparticle formation. *Physical Chemistry Chemical Physics*. 2013;**15**:1014

- [16] Cavallo D, Ciervo A, Freseghna AM, Maiello R, Tassone P, Buresti G, et al. Investigation on cobalt-oxide nanoparticles cyto-genotoxicity and inflammatory response in two types of respiratory cells. *Journal of Applied Toxicology*. 2015;**35**:1102-1113
- [17] Alarifi S, Ali D, Suliman AO, Ahamed M, Siddiqui MA, Al-Khedhairi AA. Oxidative stress contributes to cobalt oxide nanoparticles-induced cytotoxicity and DNA damage in human hepatocarcinoma cells. *International Journal of Nanomedicine*. 2013;**8**: 189-199
- [18] Syam Sundar L, Singh MK, Ferro MC, Sousa ACM. Experimental investigation of the thermal transport properties of graphene oxide/Co<sub>3</sub>O<sub>4</sub> hybrid nanofluids. *International Communications in Heat and Mass Transfer*. 2017;**84**:1-10
- [19] Syam Sundar L, Irurueta GO, Venkata Ramana E, Manoj K, Singh ACMS. Thermal conductivity and viscosity of hybrid nanofluids prepared with magnetic nanodiamond-cobalt oxide (ND-Co<sub>3</sub>O<sub>4</sub>) nanocomposite. *Case Studies in Thermal Engineering*. 2016;**7**: 66-77
- [20] Shi P, Dai X, Zheng H, Li D, Yao W, Hu C. Synergistic catalysis of Co<sub>3</sub>O<sub>4</sub> and graphene oxide on Co<sub>3</sub>O<sub>4</sub>/GO catalysts for degradation of Orange II in water by advanced oxidation technology based on sulfate radicals. *Chemical Engineering Journal*. 2014;**240**:264-270
- [21] Xiang C, Li M, Zhi M, Manivannan A, Wu N. A reduced graphene oxide/Co<sub>3</sub>O<sub>4</sub> composite for supercapacitor electrode. *Journal of Power Sources*. 2013;**226**:65-70
- [22] Liang Y, Li Y, Wang H, Zhou J, Wang J, Regier T, et al. Co<sub>3</sub>O<sub>4</sub> nanocrystals on graphene as a synergistic catalyst for oxygen reduction reaction. *Nature Materials*. 2011;**10**: 780-786
- [23] Lai L, Zhu J, Li Z, Yu DYW, Jiang S, Cai X, et al. Co<sub>3</sub>O<sub>4</sub>/nitrogen modified graphene electrode as Li-ion battery anode with high reversible capacity and improved initial cycle performance. *Nano Energy*. 2014;**3**:134-143
- [24] Syam Sundar L, Anjum NA, Ferro MC, Pereira E, Singh MK, Sousa ACM. Biocompatibility and biotoxicity of in-situ synthesized carboxylated nanodiamond-cobalt oxide nanocomposite. *Journal of Materials Science and Technology*. 2017;**33**: 879-888
- [25] Davar F, Fereshteh Z, Razavi HS, Razavi RS, Loghman-Estarki MR. Synthesis and characterization of cobalt oxide nanocomposite based on the Co<sub>3</sub>O<sub>4</sub>-zeolite Y. *Superlattices and Microstructures*. 2014;**66**:85-95
- [26] Abdolmaleki A, Kazerooni H, Gholivand MB, Heydari H, Pendashteh A. Facile electrostatic coprecipitation of f-SWCNT/Co<sub>3</sub>O<sub>4</sub> nanocomposite as supercapacitor material. *Ionic*s. 2015;**21**:515-523
- [27] Zarnegar Z, Safari J, Kafroudi ZM. Co<sub>3</sub>O<sub>4</sub>-CNT nanocomposites: A powerful, reusable, and stable catalyst for sonochemical synthesis of polyhydroquinolines. *New Journal of Chemistry*. 2015;**39**:1445-1451